

## SUPPORTING INFORMATION

### Brownian dynamics via the Langevin equation

In this model, F-actins are simplified into serially connected cylindrical segments. Each segment has polarity with barbed and pointed ends (Fig. S1a). ACPs consist of a pair of cylindrical segments. Motors are modeled as a structure with one arm. This means that one motor can bind to only one F-actin. To mimic the motility assay, motors are disallowed to move. Displacements of segments for F-actin and ACP are governed by the Langevin equation with inertia neglected:

$$\mathbf{F}_i - \zeta_i \frac{d\mathbf{r}_i}{dt} + \mathbf{F}_i^T = 0 \quad (\text{S1})$$

where  $\mathbf{r}_i$  is position of the  $i$ th element,  $\zeta_i$  is a drag coefficient,  $t$  is time,  $\mathbf{F}_i$  is a deterministic force, and  $\mathbf{F}_i^T$  is a stochastic force that satisfies the fluctuation-dissipation theorem<sup>1</sup>:

$$\langle \mathbf{F}_i^T(t) \mathbf{F}_j^T(t) \rangle = \frac{2k_B T \zeta_i \delta_{ij}}{\Delta t} \boldsymbol{\delta} \quad (\text{S2})$$

where  $\delta_{ij}$  is the Kronecker delta,  $\boldsymbol{\delta}$  is a second-order tensor, and  $\Delta t$  is a time step. In most simulations,  $\Delta t$  is  $1.5 \times 10^{-5}$  s.

Drag coefficients are computed using an approximated form for a cylindrical object<sup>2</sup>:

$$\zeta_i = 3\pi\mu r_{c,i} \frac{3 + 2r_{0,i} / r_{c,i}}{5} \quad (\text{S3})$$

where  $\mu$  is viscosity of medium, and  $r_{0,i}$  and  $r_{c,i}$  are length and diameter of a segment, respectively. Positions of cylindrical segments for F-actin and ACP at each time step are updated using the Euler integration scheme:

$$\mathbf{r}_i(t + \Delta t) = \mathbf{r}_i(t) + \frac{d\mathbf{r}_i}{dt} \Delta t = \mathbf{r}_i(t) + \frac{1}{\zeta_i} (\mathbf{F}_i + \mathbf{F}_i^T) \Delta t \quad (\text{S4})$$

### Deterministic forces

Deterministic forces include i) extensional forces that maintain the equilibrium lengths of segments, ii) bending forces that maintain the equilibrium angles between interconnected segments, and iii) repulsive forces that account for volume-exclusion effects between neighboring actin segments. The extensional and bending forces originate from harmonic potentials:

$$U_s = \frac{1}{2} \kappa_s (r - r_0)^2 \quad (\text{S5})$$

$$U_b = \frac{1}{2} \kappa_b (\theta - \theta_0)^2 \quad (\text{S6})$$

where  $\kappa_s$  is extensional stiffness,  $r$  and  $r_0$  are instantaneous and equilibrium lengths of segments,  $\kappa_b$  is bending stiffness, and  $\theta$  and  $\theta_0$  are instantaneous and equilibrium angles formed by interconnected adjacent segments. Extensional ( $\kappa_{s,A}$ ) and bending ( $\kappa_{b,A}$ ) stiffnesses of F-actin control an equilibrium length of actin segments ( $r_{0,A} = 140$  nm) and an equilibrium angle formed by two adjacent actin segments ( $\theta_{0,A} = 0$  rad), respectively. With the reference value of  $\kappa_{b,A}$ , persistence length of F-actin is  $\sim 9$   $\mu\text{m}$ .<sup>3</sup> Extensional ( $\kappa_{s,ACP}$ ) and bending ( $\kappa_{b,ACP}$ ) stiffnesses of ACP maintain an equilibrium length of an ACP segment ( $r_{0,ACP} = 23.5$  nm) and an equilibrium angle formed by two ACP segments ( $\theta_{0,ACP} = 0$  rad), respectively. Geometry of ACPs resembles that of  $\alpha$ -actinin.<sup>4</sup> Extensional stiffness of motors ( $\kappa_{s,M}$ ) maintains an equilibrium length of a motor segment ( $r_{0,M} = 13.5$  nm). Forces exerted on actin segments by bound ACPs and motors are distributed to the barbed and pointed ends of the actin segments as described in our previous work.<sup>5</sup>

## Actin dynamics

The formation of F-actin is initiated by a nucleation event with the appearance of one cylindrical segment with polarity within the computational domain in a random direction perpendicular to the  $z$  direction. Polymerization of actin is simulated by the addition of one cylindrical segment. Depolymerization of actin is not considered, therefore if all actin segments are used for the nucleation and polymerization, there is no more change in the length of each F-actin.

## Dynamic behaviors of ACPs

ACP binds to binding sites located every 7 nm on actin segments with no preference of contact angle. ACPs unbind from F-actin in a force-dependent manner, following Bell's law<sup>7</sup>:

$$k_{u,ACP} = \begin{cases} k_{u,ACP}^0 \exp\left(\frac{\lambda_{u,ACP} |\vec{F}_{s,ACP}|}{k_B T}\right) & \text{if } r \geq r_{0,ACP} \\ k_{u,ACP}^0 & \text{if } r < r_{0,ACP} \end{cases} \quad (\text{S7})$$

where  $k_{u,ACP}^0$  is a zero-force unbinding rate constant,  $\lambda_{u,ACP}$  represents sensitivity to the magnitude of applied spring force, and  $k_B T$  is thermal energy. Reference values of  $k_{u,ACP}^0$  ( $= 0.115 \text{ s}^{-1}$ ) and  $\lambda_{u,ACP}$  ( $= 1.04 \times 10^{-10} \text{ m}$ ) are determined based on filamin A.<sup>8</sup>

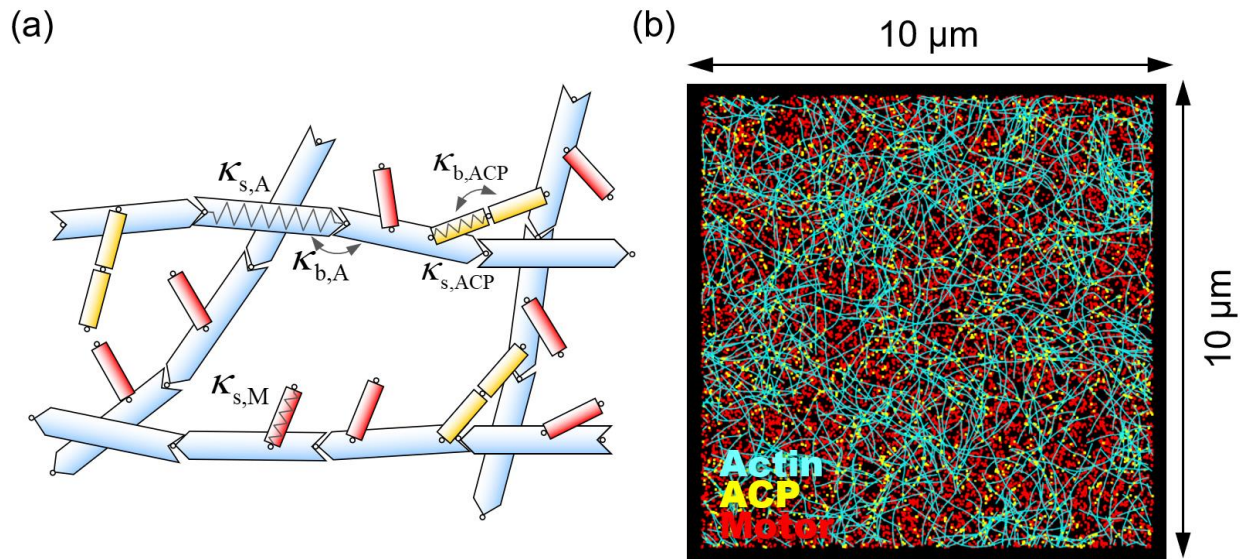


**Figure S1. Agent-based computational model used for simulations in this study.** (a) A schematic diagram showing a network consisting of F-actin (cyan), actin cross-linking protein (ACP, yellow), and motor (red). Each element is simplified by cylindrical segments. Bending ( $\kappa_b$ ) and extensional stiffnesses ( $\kappa_s$ ) maintain equilibrium angles formed by adjacent cylindrical segments (indicated by bent arrows) and equilibrium lengths of cylindrical segments (indicated by springs), respectively. (b) An example of networks formed by self-assembly of the three elements in a very thin computational domain ( $10 \times 10 \times 0.1 \mu\text{m}$ ) with a periodic boundary condition in x and y directions.

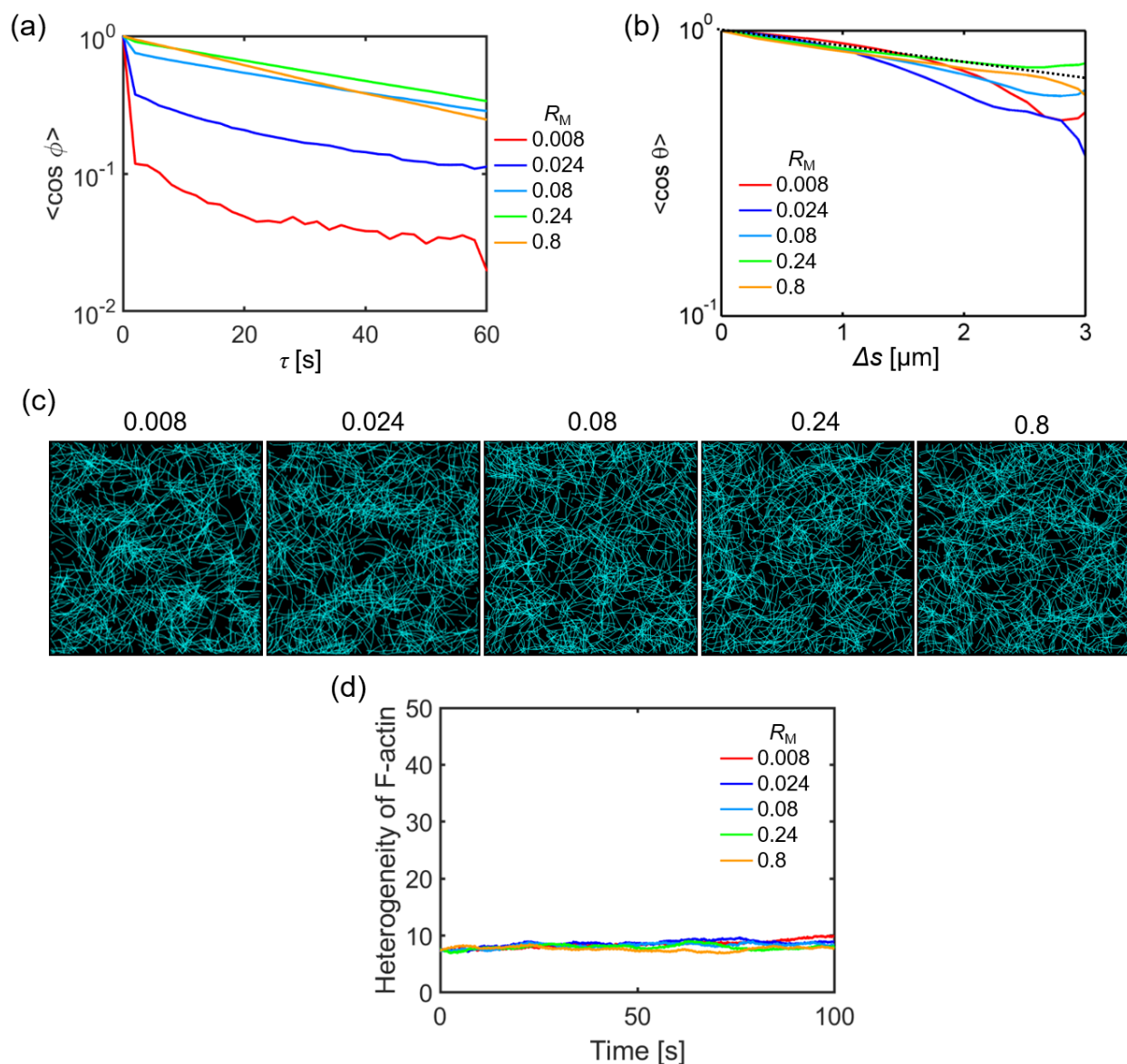


**Figure S2. Effects of motor density ( $R_M$ ).** (a) Autocorrelation of velocities of F-actins with various  $R_M$ . With smaller  $R_M$ , persistency of F-actin movement tends to be lower due to a larger number of free F-actins and F-actins bound to only one motor. (b) A correlation between unit tangential vectors along contour of F-actins. A dotted line indicates the correlation corresponding to the persistence length of F-actin. (c) Morphology of networks with different  $R_M$  at the last time point,  $t = 100$  s. (d) Heterogeneity of F-actin spatial distribution ( $Q_A$ ).  $R_M$  hardly affects the heterogeneity.

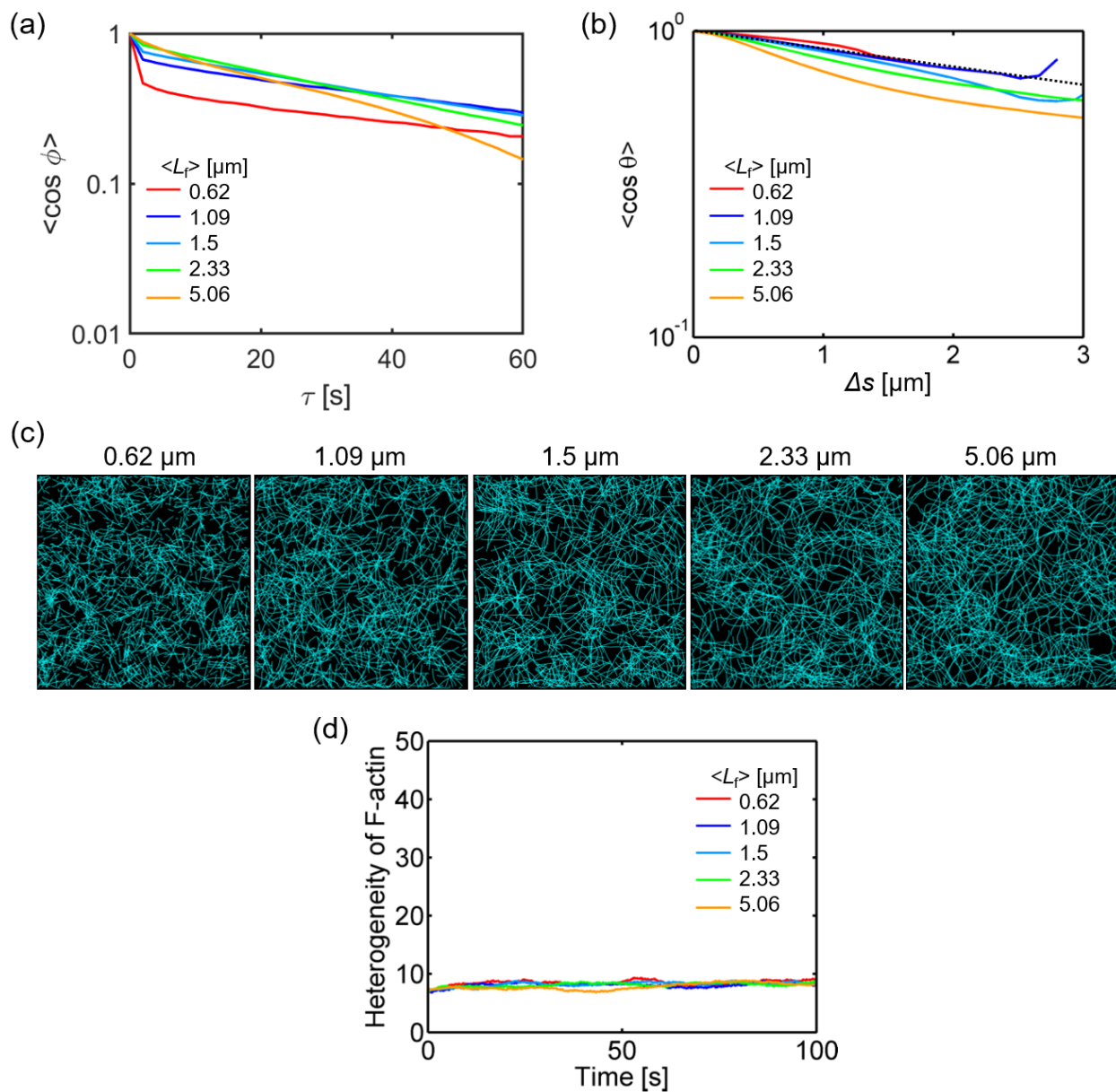


**Figure S3. Influences of average length of F-actins ( $\langle L_f \rangle$ ).** (a) Autocorrelation of velocities of F-actins. (b) A correlation between unit tangential vectors along contour of F-actins. A dotted line indicates the correlation corresponding to the persistence length of F-actin. With lower  $\langle L_f \rangle$ , F-actins are less curvy because of a larger number of free F-actins and F-actins bound to only one motor. (c) Morphology of networks with various  $\langle L_f \rangle$  at the last time point,  $t = 100$  s. (d) Heterogeneity of spatial distribution of F-actins ( $Q_A$ ). In all cases, networks are very homogeneous.

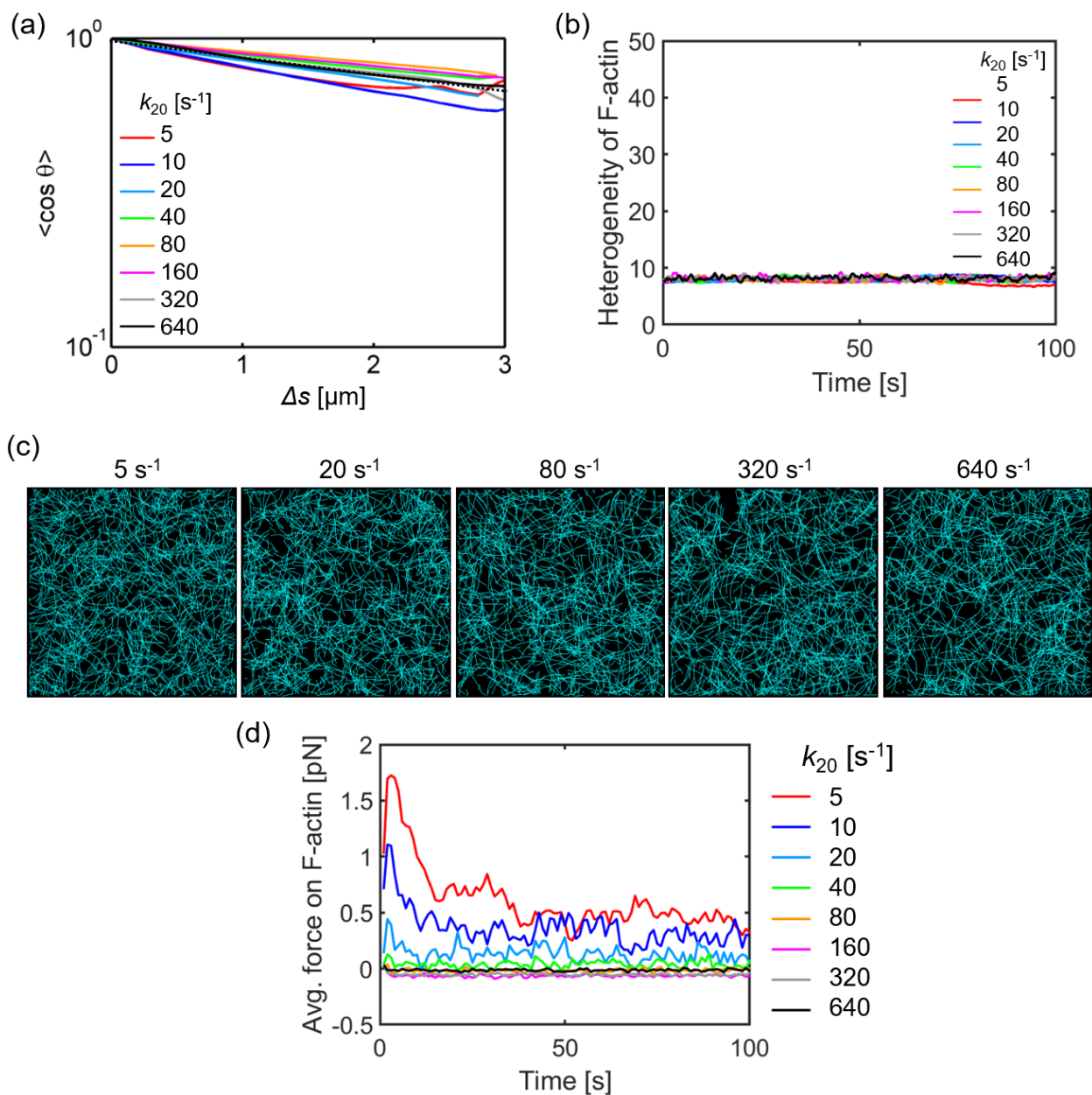


**Figure S4. Influences of one of mechanochemical rates of myosin heads employed in the parallel cluster model, the ATP-dependent unbinding rate of motors ( $k_{20}$ ).** (a) A correlation between unit tangential vectors along contour of F-actin. A dotted line indicates the correlation corresponding to the persistence length of F-actin. (b) Heterogeneity of F-actin spatial distribution ( $Q_A$ ). (c) Morphology of networks with various  $k_{20}$  at the last time point,  $t = 100$  s. Networks are quite homogeneous, regardless of  $k_{20}$ . (d) Average tensile force exerted on F-actins. Motors with lower  $k_{20}$  exert slightly larger forces on F-actins due to higher stall force.

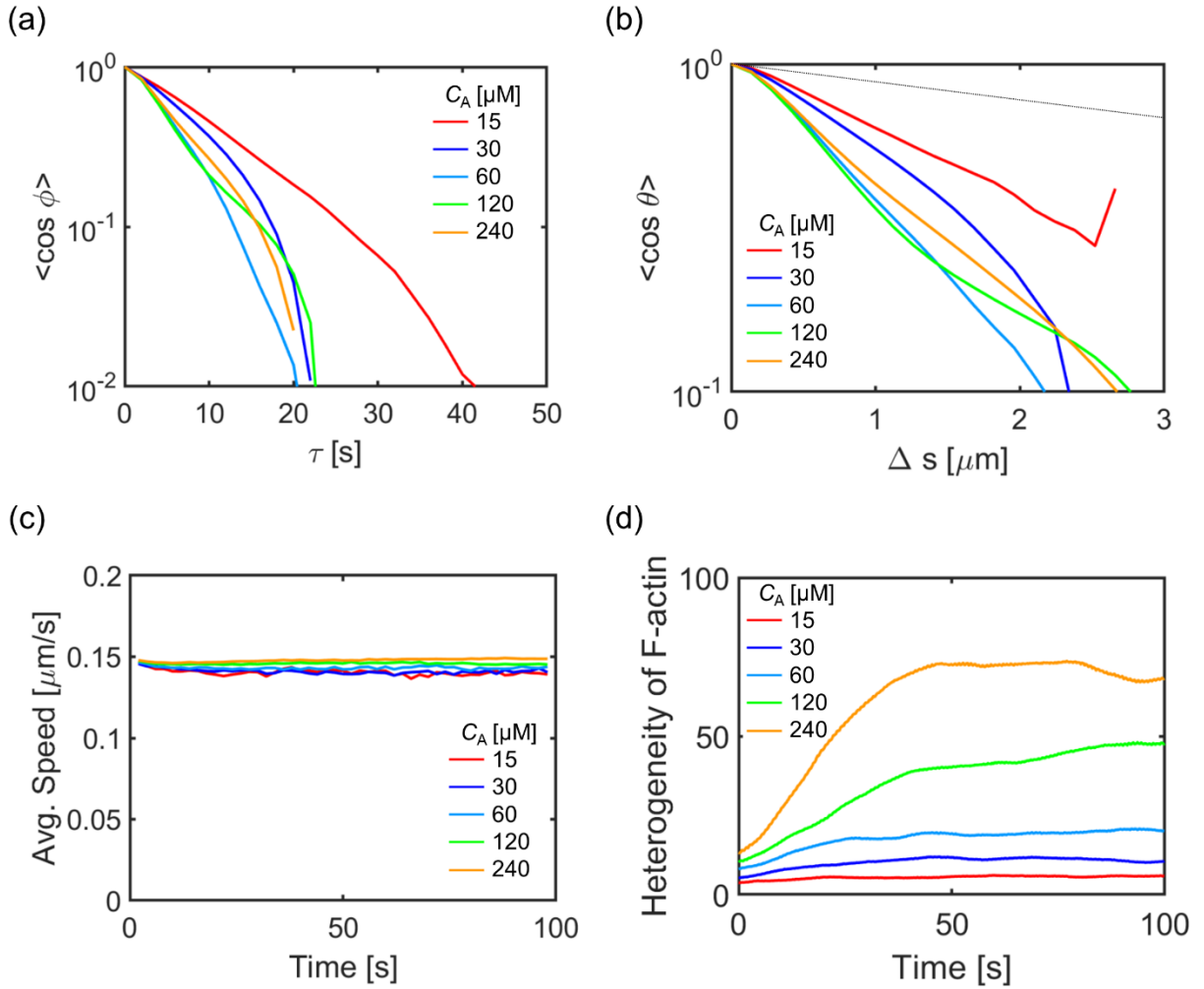


**Figure S5. Effects of actin concentration ( $C_A$ ) on motions of F-actins and network morphology in the presence of volume-exclusion effects ( $\kappa_{r,A} = \kappa_{r,A}^*$ ).** (a) Autocorrelation of velocities of F-actins with various  $C_A$ . (b) A correlation between unit tangential vectors along contour of F-actins. A dotted line indicates the correlation corresponding to the persistence length of F-actin. (c) Average speed of F-actins. (d) Heterogeneity of F-actin spatial distribution ( $Q_A$ ).

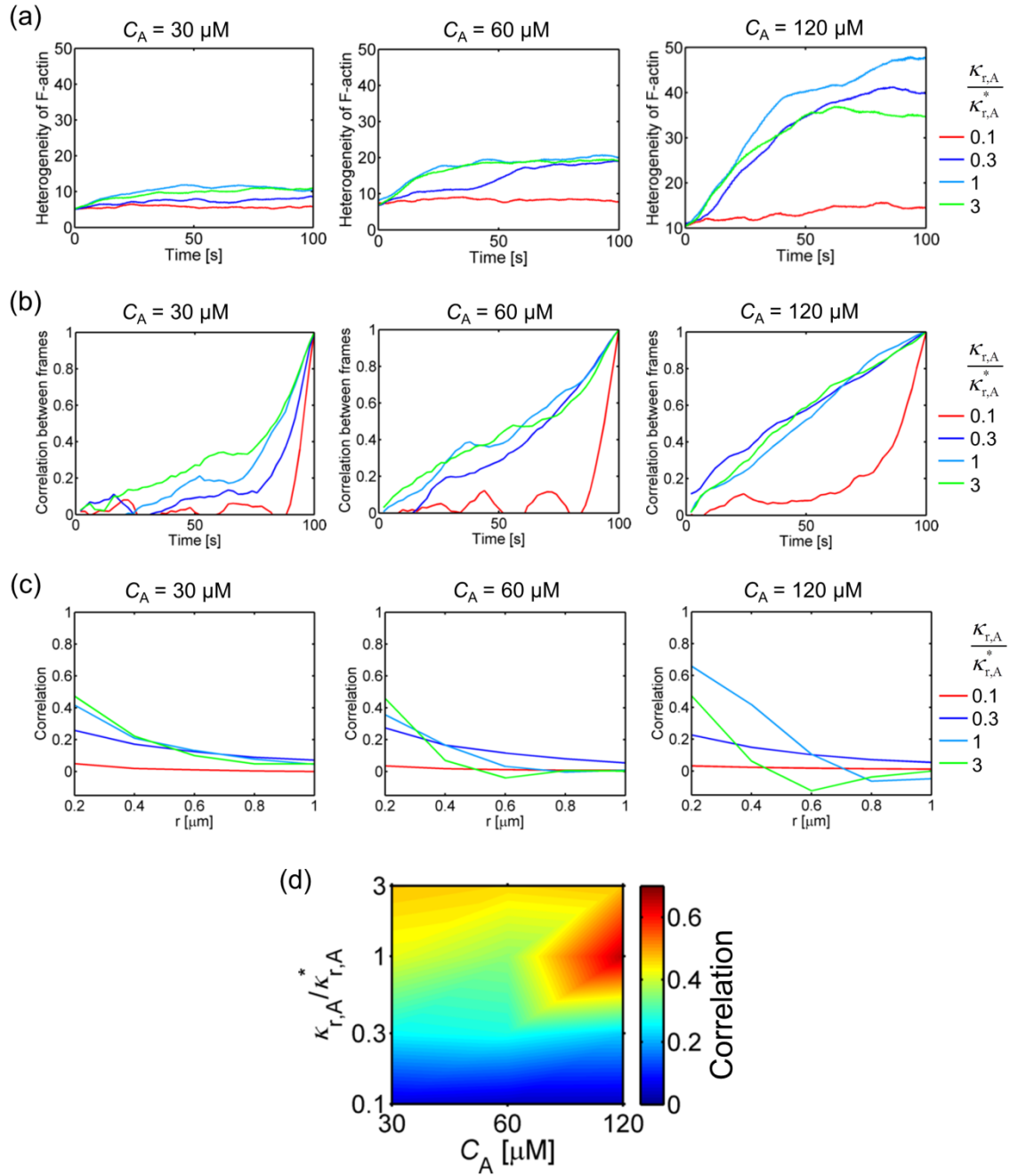


**Figure S6. Impacts of the extent of volume-exclusion effects on network morphology and collective motions of F-actins with three different actin concentrations ( $C_A = 30, 60,$  and  $120 \mu\text{M}$ ).** (a) Heterogeneity of F-actin spatial distribution ( $Q_A$ ). (b) A correlation between final network morphology at 100 s and morphology at each time point,  $t$ . (c-d) A correlation between velocities of two points on different F-actins located (c) near a distance  $r$  or (d) within  $0.2 \mu\text{m}$ . The correlation values are averaged for last 50 s.

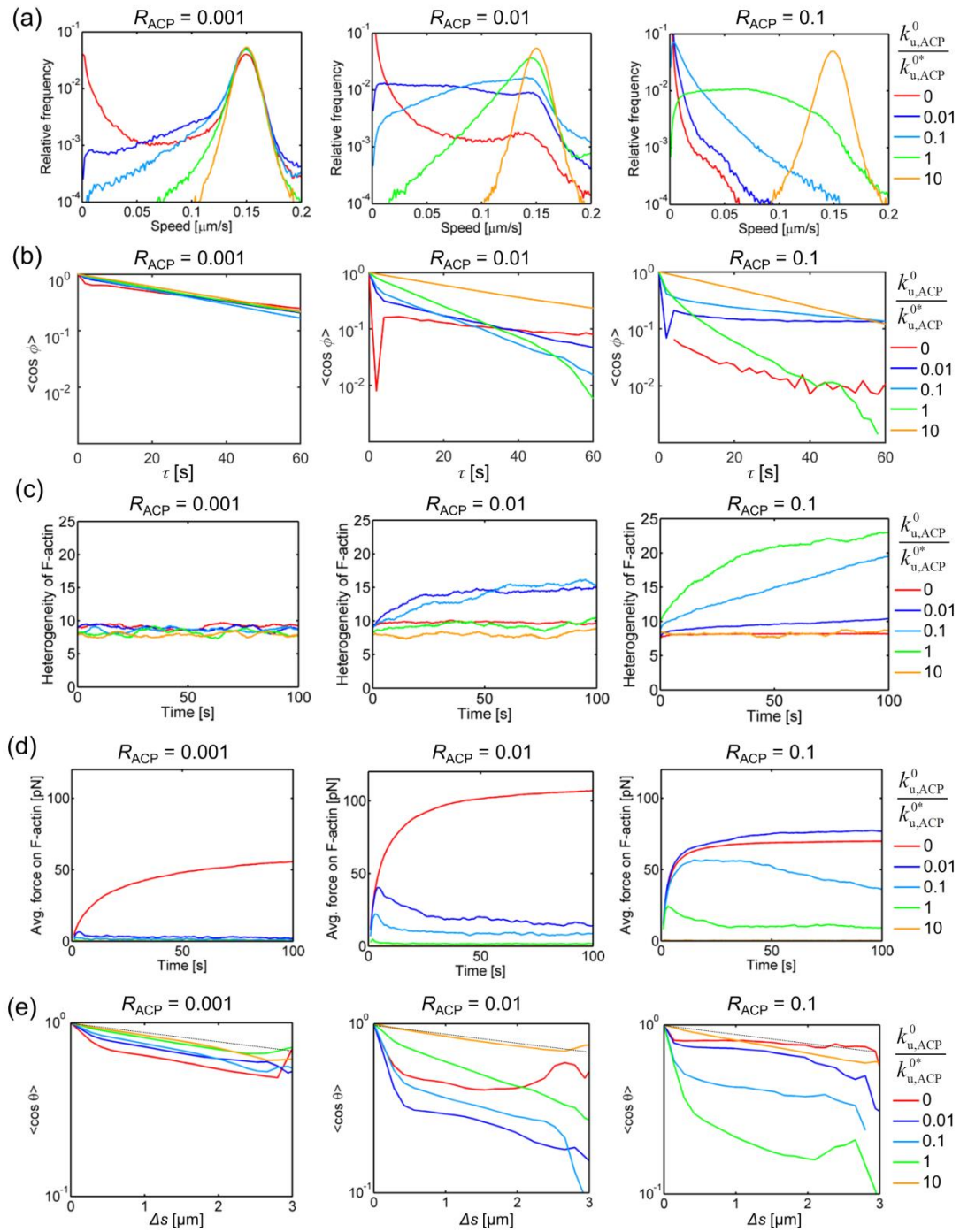


**Figure S7. Influences of density ( $R_{ACP}$ ) and zero-force unbinding rate constant ( $k_{u,ACP}^0$ ) of ACPs.** (a) Speed distribution of F-actins. (b) Autocorrelation of velocities of F-actins. A spike at low  $\tau$  in some curves originates from severe confinement of F-actins. (c) Heterogeneity of F-actin spatial distribution ( $Q_A$ ). (d) Time evolution of average tensile force acting on F-actins. (e) A correlation between unit tangential vectors along contour of F-actins. Dotted lines indicate the correlation corresponding to the persistence length of F-actin.

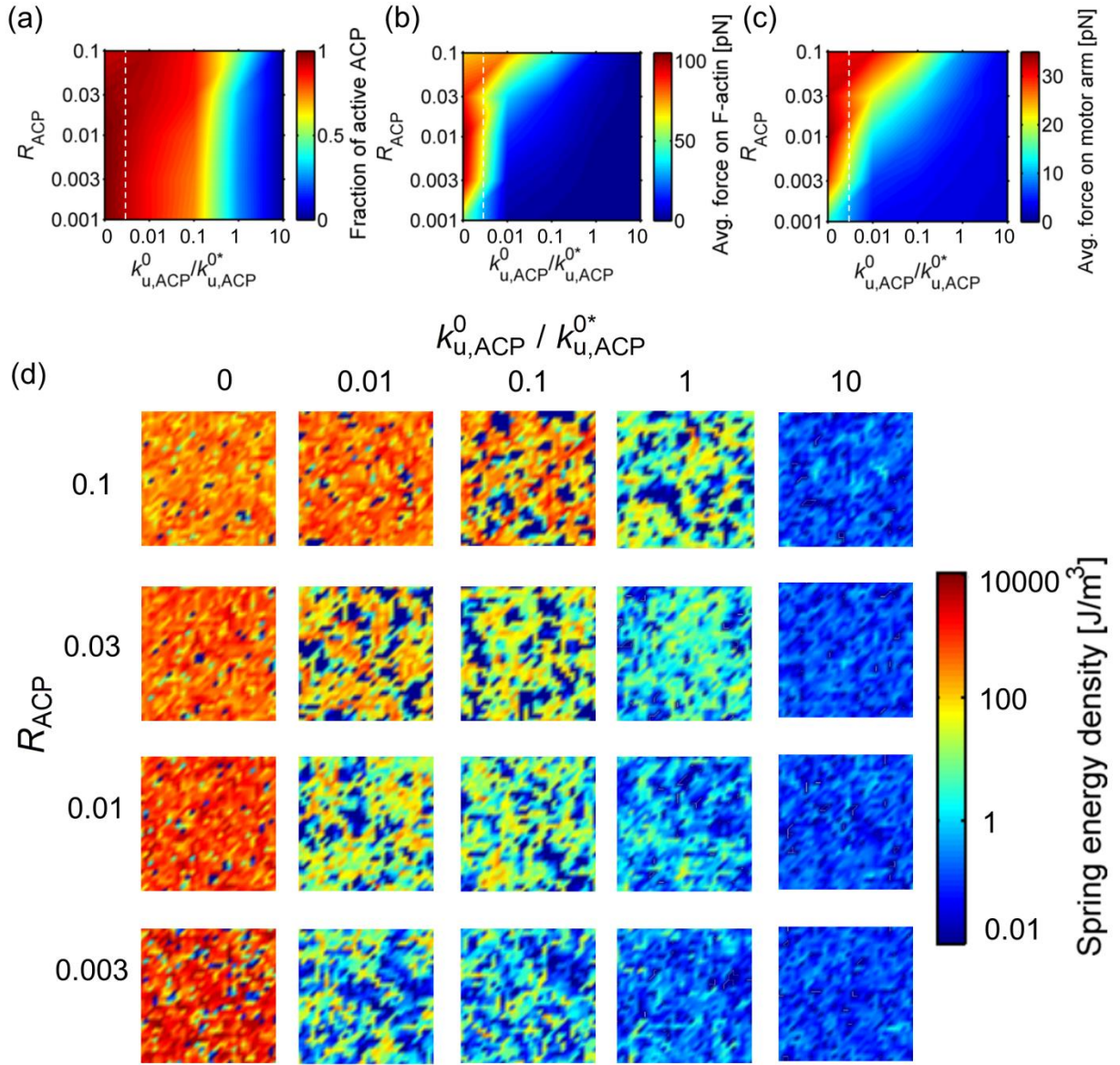


**Figure S8. Effects of the density ( $R_{ACP}$ ) and zero-force unbinding rate constant ( $k_{u,ACP}^0$ ) of ACPs.** (a) The fraction of active ACPs with various  $R_{ACP}$  and  $k_{u,ACP}^0$ , which is equal to the ratio of density of active ACPs bound to pairs of F-actins ( $R_{ACP}^{active}$ ) to density of all ACPs ( $R_{ACP}$ ). The fraction was averaged for last 50 s.  $k_{u,ACP}^{0*} = 0.115 \text{ s}^{-1}$  is the reference value of  $k_{u,ACP}^0$ . (b) Tensile force acting on F-actins averaged for last 50 s. (c) Force exerted by motor arms averaged for last 50 s. White dashed lines in (a-c) are drawn to include cases with  $k_{u,ACP}^0 = 0$  in a log scale, so there is discontinuity between cases with  $k_{u,ACP}^0/k_{u,ACP}^{0*} = 0$  and those with  $k_{u,ACP}^0/k_{u,ACP}^{0*} = 0.01$ . (d) Visualization of spatial distribution of spring energy density in networks measured at  $t = 100 \text{ s}$  via color scaling.

**Table S1. List of parameters employed in the model.** For some of the parameters, references are provided if the parameters were determined based on specific previous studies.

Symbol	Definition	Value
$r_{0,A}$	Length of an actin segment	$1.4 \times 10^{-7}$ [m]
$r_{c,A}$	Diameter of an actin segment	$7.0 \times 10^{-9}$ [m] <sup>9</sup>
$\theta_{0,A}$	Bending angle formed by adjacent actin segments	0 [rad]
$\kappa_{s,A}$	Extensional stiffness of F-actin	$1.69 \times 10^{-2}$ [N/m]
$\kappa_{b,A}^*$	Reference bending stiffness of F-actin	$2.64 \times 10^{-19}$ [N·m] <sup>3</sup>
$r_{0,ACP}$	Length of an ACP arm	$2.35 \times 10^{-8}$ [m] <sup>10</sup>
$r_{c,ACP}$	Diameter of an ACP arm	$1.0 \times 10^{-8}$ [m]
$\theta_{0,ACP}$	Bending angle formed by two ACP arms	0 [rad]
$\kappa_{s,ACP}$	Extensional stiffness of ACP	$2.0 \times 10^{-3}$ [N/m]
$\kappa_{b,ACP}$	Bending stiffness of ACP	$1.04 \times 10^{-19}$ [N·m]
$r_{0,M}$	Length of a motor arm	$1.35 \times 10^{-8}$ [m]
$r_{c,M}$	Diameter of a motor arm	$1.0 \times 10^{-8}$ [m]
$\kappa_{s,M}$	Extensional stiffness of a motor arm	$1.0 \times 10^{-3}$ [N/m]
$k_{20}^*$	Reference ATP-dependent unbinding rate of myosin heads	20 [s <sup>-1</sup> ]
$N_h$	Number of heads represented by a motor arm	8
$N_a$	Number of arms in a motor	1
$k_{n,A}$	Nucleation rate of actin	$0.000125 - 1$ [ $\mu\text{M}^{-1}\text{s}^{-1}$ ]
$k_{+,A}$	Polymerization rate of actin at the barbed end	60 [ $\mu\text{M}^{-1}\text{s}^{-1}$ ]
$k_{u,ACP}^{0*}$	Reference zero-force unbinding rate constant of ACP	$0.115$ [s <sup>-1</sup> ] <sup>8</sup>
$\lambda_{u,ACP}$	Sensitivity of ACP unbinding to an applied force	$1.04 \times 10^{-10}$ [m] <sup>8</sup>
$\kappa_{r,A}^*$	Reference strength of a repulsive force	$1.69 \times 10^{-3}$ [N/m]
$\Delta t$	Time step	$1.15 \times 10^{-5}$ [s]
$\mu$	Viscosity of surrounding medium	$8.6 \times 10^{-1}$ [kg/m·s]
$k_B T$	Thermal energy	$4.142 \times 10^{-21}$ [J]
$C_A$	Actin concentration	15 – 240 [ $\mu\text{M}$ ]
$R_M$	Motor density (= Ratio of motor concentration to $C_A$ )	0.008 – 0.8
$R_{ACP}$	ACP density (= Ratio of ACP concentration to $C_A$ )	0 – 0.1
$\langle L_{\bar{r}} \rangle$	Average length of F-actins	0.62 – 5.06 [ $\mu\text{m}$ ]

**Table S2. List of parameter values used for adopting “parallel cluster model.”<sup>11, 12</sup>** Note that we used slightly different values for  $F_0$ ,  $d$ , and  $k_m$  from those in the literature.

<b>Symbol</b>	<b>Definition</b>	<b>Value</b>
$k_{01}$	A rate from unbound to weakly bound state	40 [s <sup>-1</sup> ]
$k_{10}$	A rate from weakly bound to unbound state	2 [s <sup>-1</sup> ]
$k_{12}$	A rate from weakly bound to post-power-stroke state	1000 [s <sup>-1</sup> ]
$k_{21}$	A rate from post-power-stroke to weakly bound state	1000 [s <sup>-1</sup> ]
$k_{20}$	A rate from post-power-stroke to unbound state	5-640 [s <sup>-1</sup> ]
$F_0$	Constant for force dependence	$5.04 \times 10^{-12}$ [N]
$E_{pp}$	Free energy bias toward the post-power-stroke state	$-60 \times 10^{-21}$ [J]
$E_{ext}$	External energy contribution	0 [J]
$d$	Step size	$7 \times 10^{-9}$ [m]
$k_m$	Spring constant of the neck linkers	$1.0 \times 10^{-3}$ [N/m] (= $\kappa_{s,M}$ )

## MOVIE CAPTIONS

**Movie S1. Motions of F-actins under a reference condition in the absence of ACPs and volume-exclusion effects between F-actins** ( $\kappa_{r,A} = 0$ ,  $\langle L_f \rangle = 1.5 \mu\text{m}$ ,  $R_M = 0.8$ ,  $k_{20} = 20 \text{ s}^{-1}$ ,  $R_{ACP} = 0$ ,  $C_A = 60 \mu\text{M}$ ). F-actins and motors are visualized by cyan and red, respectively. Duration of the movie is 100 s.

**Movie S2. Collective motions of F-actins with various actin concentration ( $C_A$ ) in the presence of volume-exclusion effects between F-actins without ACPs** ( $\kappa_{r,A} / \kappa_{r,A}^* = 1$ ,  $\langle L_f \rangle = 1.5 \mu\text{m}$ ,  $R_M = 0.8$ ,  $k_{20} = 20 \text{ s}^{-1}$ ,  $R_{ACP} = 0$ ).  $C_A$  in the left, center, and right is 15, 60, and 120  $\mu\text{M}$ , respectively. F-actins are visualized by different colors to show their dynamic motions. Duration of the movie is 100 s.

**Movie S3. Collective motions of F-actins with different extents of volume-exclusion effects between F-actins in the absence of ACPs** ( $\langle L_f \rangle = 1.5 \mu\text{m}$ ,  $R_M = 0.8$ ,  $k_{20} = 20 \text{ s}^{-1}$ ,  $R_{ACP} = 0$ ,  $C_A = 60 \mu\text{M}$ ). The relative strength of volume-exclusion effects ( $\kappa_{r,A} / \kappa_{r,A}^*$ ) in the left, center, and right is 0.3, 1, and 3, respectively. F-actins are visualized by different colors to show their dynamic motions. Duration of the movie is 100 s.

**Movie S4. Movements of F-actins with transient ACPs in the absence of volume-exclusion effects between F-actins** ( $\kappa_{r,A} = 0$ ,  $\langle L_f \rangle = 1.5 \mu\text{m}$ ,  $R_M = 0.8$ ,  $k_{20} = 20 \text{ s}^{-1}$ ,  $R_{ACP} = 0.1$ ,  $k_{u,ACP}^0 / k_{u,ACP}^{0*} = 1$ ,  $C_A = 60 \mu\text{M}$ ). F-actins and ACPs are visualized by cyan and yellow, respectively. Duration of the movie is 100 s.

**Movie S5. Motions of F-actins with much less transient ACPs in the absence of volume-exclusion effects between F-actins** ( $\kappa_{r,A} = 0$ ,  $\langle L_f \rangle = 1.5 \mu\text{m}$ ,  $R_M = 0.8$ ,  $k_{20} = 20 \text{ s}^{-1}$ ,  $R_{ACP} = 0.1$ ,  $k_{u,ACP}^0 / k_{u,ACP}^{0*} = 0.01$ ,  $C_A = 60 \mu\text{M}$ ). F-actins and ACPs are visualized by cyan and yellow, respectively. Duration of the movie is 100 s.

## REFERENCES

1. P. T. Underhill and P. S. Doyle, *J. Non-Newton. Fluid.*, 2004, **122**, 3-31.
2. R. Clift, J. R. Grace and M. E. Weber, *Bubbles, drops, and particles*, Courier Corporation, 2005.
3. H. Isambert, P. Venier, A. C. Maggs, A. Fattoum, R. Kassab, D. Pantaloni and M. F. Carlier, *J. Biol. Chem.*, 1995, **270**, 11437-11444.
4. S. Le, X. Hu, M. Yao, H. Chen, M. Yu, X. Xu, N. Nakazawa, F. M. Margadant, M. P. Sheetz and J. Yan, *Cell Rep.*, 2017, **21**, 2714-2723.
5. T. Kim, *Biomech. Model. Mechanobiol.*, 2015, **14**, 345-355.
6. T. Kim, W. Hwang, H. Lee and R. D. Kamm, *PLoS Comput. Biol.*, 2009, **5**, e1000439.
7. G. I. Bell, *Science*, 1978, **200**, 618-627.
8. J. M. Ferrer, H. Lee, J. Chen, B. Pelz, F. Nakamura, R. D. Kamm and M. J. Lang, *Proc. Natl. Acad. Sci. U. S. A.*, 2008, **105**, 9221-9226.
9. A. Kishino and T. Yanagida, *Nature*, 1988, **334**, 74-76.
10. R. K. Meyer and U. Aebi, *J. Cell Biol.*, 1990, **110**, 2013-2024.
11. T. Erdmann, P. J. Albert and U. S. Schwarz, *J. Chem. Phys.*, 2013, **139**, 175104.
12. T. Erdmann and U. S. Schwarz, *Phys. Rev. Lett.*, 2012, **108**, 188101.